AAC Journals.ASM.org

Severe Acute Respiratory Syndrome Coronavirus Replication Inhibitor That Interferes with the Nucleic Acid Unwinding of the Viral Helicase

Adeyemi O. Adedeji,[a] Kamalendra Singh,[a] Nicholas E. Calcaterra,[a,b] Marta L. DeDiego,[c] Luis Enjuanes,[c] Susan Weiss,[d] and Stefan G. Sarafianos[a,b]

Christopher S. Bond Life Sciences Center, Department of Molecular Microbiology and Immunology, University of Missouri School of Medicine,[a] and Department of Biochemistry, University of Missouri,[b] Columbia, Missouri, USA; Centro Nacional de Biotecnología-CSIC Spanish Council for Scientific Research, Campus Universidad Autónoma, Madrid, Spain[c]; and Department of Microbiology, University of Pennsylvania, School of Medicine, Philadelphia, Pennsylvania, USA[d]

Severe acute respiratory syndrome (SARS) is a highly contagious disease, caused by SARS coronavirus (SARS-CoV), for which there are no approved treatments. We report the discovery of a potent inhibitor of SARS-CoV that blocks replication by inhibiting the unwinding activity of the SARS-CoV helicase (nsp13). We used a Förster resonance energy transfer (FRET)-based helicase assay to screen the Maybridge Hitfinder chemical library. We identified and validated a compound (SSYA10-001) that specifically blocks the double-stranded RNA (dsRNA) and dsDNA unwinding activities of nsp13, with 50% inhibitory concentrations (IC_{50}s) of 5.70 and 5.30 μM, respectively. This compound also has inhibitory activity (50% effective concentration [EC_{50}] = 8.95 μM) in a SARS-CoV replicon assay, with low cytotoxicity (50% cytotoxic concentration [CC_{50}] = >250 μM), suggesting that the helicase plays a still unidentified critical role in the SARS-CoV life cycle. Enzyme kinetic studies on the mechanism of nsp13 inhibition revealed that SSYA10-001 acts as a noncompetitive inhibitor of nsp13 with respect to nucleic acid and ATP substrates. Moreover, SSYA10-001 does not affect ATP hydrolysis or nsp13 binding to the nucleic acid substrate. SSYA10-001 did not inhibit hepatitis C virus (HCV) helicase, other bacterial and viral RNA-dependent RNA polymerases, or reverse transcriptase. These results suggest that SSYA10-001 specifically blocks nsp13 through a novel mechanism and is less likely to interfere with the functions of cellular enzymes that process nucleic acids or ATP. Hence, it is possible that SSYA10-001 inhibits unwinding by nsp13 by affecting conformational changes during the course of the reaction or translocation on the nucleic acid. SSYA10-001 will be a valuable tool for studying the specific role of nsp13 in the SARS-CoV life cycle, which could be a model for other nidoviruses and also a candidate for further development as a SARS antiviral target.

Severe acute respiratory syndrome coronavirus (SARS-CoV) is responsible for the life-threatening viral respiratory illness known as SARS, which emerged from Southern China in November 2002 and spread to other parts of the world, including North America, South America, and Europe (50, 64). There is currently no approved therapeutic agent for the treatment of SARS-CoV infections. Although SARS currently does not pose a public health threat, the likelihood of future occurrences of both SARS-CoV and related viruses necessitates continuous research for identification of antiviral therapies.

SARS-CoV contains a single-stranded, 5′-capped, polyadenylated positive-strand RNA genome that is ~29.7 kb long (40, 45). The first open reading frame (ORF1a/b) encompasses about two-thirds of the genome and codes for the replicase proteins (41). Following a −1 frameshift signal, translation continues in ORF1b after initiation at ORF1a. The virally encoded chymotrypsin-like protease $3CL^{pro}$ (also called M^{pro} or main protease) and the papain-like protease (PLP) cleave (by autoproteolysis) the newly formed ORF1a and ORF1ab polypeptides, i.e., pp1a and pp1ab, respectively, into 16 nonstructural proteins, including an NTPase/helicase that is known as nonstructural protein 13 (nsp13). Helicases are potential targets for antiviral therapies, as they have been reported to be indispensable for viral genome replication (5, 7, 12, 16, 25, 52, 60, 63, 65, 70, 73).

We previously performed a detailed biochemical characterization of SARS-CoV helicase (2); our results showed that this enzyme exhibits a kinetic step size of 9.3 bp/step, while unwinding nucleic acid at a rate of ~280 bp s^{-1}. It has also been shown that the SARS-CoV helicase possesses an RNA 5′-triphosphatase activity that may be involved in capping of viral RNA (20). Other studies have previously identified potential inhibitors of nsp13. Some of these inhibitors interfere with the unwinding and ATPase activities of nsp13 (23, 31, 62). Such inhibitors may also interfere with the ATPase activity of cellular ATPase or kinases and affect cellular activities. A recent study reported that an aryl diketoacid compound selectively inhibited the duplex DNA unwinding activity of SARS-CoV nsp13. However, the effects of this compound on nsp13's unwinding activity toward double-stranded RNA (dsRNA) and the replication of SARS-CoV were not determined (31).

Here we identified a potent inhibitor of nsp13 that inhibits the unwinding but not the ATPase enzymatic and nucleic acid binding activities of nsp13. We used a Förster resonance energy transfer (FRET)-based microplate screening assay to screen the Maybridge Hitfinder chemical library for potential inhibitors. Using biochemical analyses, we demonstrated that this compound, SSYA10-001, is a noncompetitive inhibitor of nsp13 with respect to its major substrates, namely, nucleic acids and ATP. Moreover, SSYA10-001 is an efficient inhibitor of viral replication, as demonstrated in a SARS-CoV replicon assay.

Received 8 May 2012 Returned for modification 30 May 2012
Accepted 14 June 2012
Published ahead of print 25 June 2012
Address correspondence to Stefan G. Sarafianos, sarafianoss@missouri.edu.

doi:10.1128/AAC.00957-12

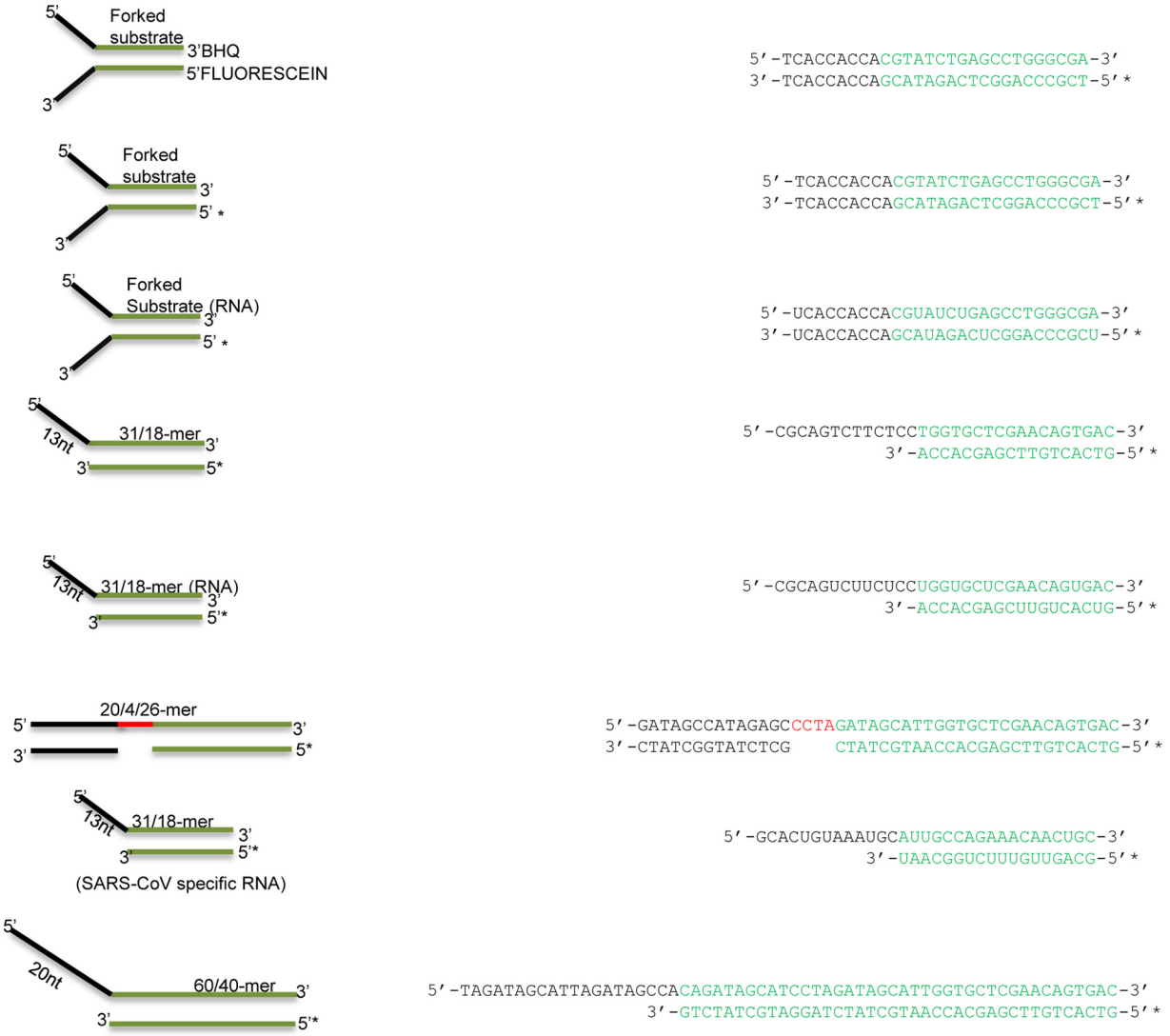

FIG 1 Oligonucleotides and substrates used in this study. The Cy3-labeled strands are marked by asterisks. The sequences in green denote complementary sequences, while the sequences in black denote noncomplementary sequences.

MATERIALS AND METHODS

Materials. The Maybridge Hitfinder chemical library of compounds (version 6) was purchased from Maybridge (Thermo Fisher Scientific, Cornwall, United Kingdom). Screening reactions were carried out in Microfluor 2 black U-bottom 96-well plates (Fisher Scientific). Compound hits were also purchased independently from Ryan Scientific Inc. (Mt. Pleasant, SC) for independent validation of the inhibition results. Synthetic oligonucleotides were purchased from Integrated DNA Technologies (Coralville, IA). Sequences of the DNA and/or RNA substrates are shown in Fig. 1.

Concentrations were determined spectrophotometrically, using absorption at 260 nm and chemical extinction coefficients. For the screening assay, a fluorescein-labeled oligonucleotide was annealed with a black hole quencher (BHQ)-labeled oligonucleotide at a ratio of 1:1.2 in 50 mM Tris, pH 8.0, plus 50 mM NaCl by heating at 95°C for 5 min and cooling slowly to room temperature. For the gel-based assay, an unlabeled oligonucleotide was annealed to the corresponding 5′-Cy3-labeled 28-mer oligonucleotide under similar conditions to those described previously.

Cloning, expression, and purification of nsp13. The cloning, expression, and purification of nsp13 were performed as previously described (2). Briefly, nsp13 was prepared with either a glutathione *S*-transferase (GST) or His_6 tag. GST-nsp13 was expressed in a baculovirus expression system and purified using glutathione Sepharose beads (Amersham Biosciences) followed by gel filtration using a Superdex 200 column (GE Healthcare) as we have described previously (2). The inhibitors blocked the activity of both enzymes, with the same 50% inhibitory concentration (IC_{50}).

HCV NS3h protein expression and purification. The recombinant plasmid pET21-NS3HCV was provided by Charles Rice (Rockefeller University). Expression of hepatitis C virus (HCV) NS3h in *Escherichia coli* BL21(DE3) was induced with 1 mM isopropyl-1-thio-β-D-galactopyranoside (IPTG) for 3 h at 37°C. The cells were harvested, and the cell pellet from a 1-liter culture was incubated with 40 ml lysis buffer (50 mM Tris-HCl, pH 7.8, 500 mM NaCl, 1 mM phenylmethylsulfonyl fluoride [PMSF], 0.1% NP-40, 1% sucrose, and 2 mg/ml lysozyme), sonicated, and centrifuged at 15,000 × *g* for 30 min. The supernatant was diluted 2-fold in buffer A (50 mM Tris-HCl, pH 7.8, 1 mM PMSF, 4% streptomycin sulfate, and 10% sucrose), stirred on ice for 30 min, and centrifuged. The supernatant was loaded on a Ni-nitrilotriacetic acid (Ni-NTA) column, and bound proteins were washed with 20 ml buffer B (20 mM Tris-HCl,

pH 7.5, 500 mM NaCl) and 5 mM imidazole, followed by 20 ml buffer B with 75 mM imidazole.

NS3h was eluted in 2-ml fractions with 20 ml buffer B containing 300 mM imidazole. Fractions with NS3h were pooled and further purified by size-exclusion chromatography (Superdex 75; GE Healthcare). The resulting protein was >90% pure as determined by SDS-PAGE with Coomassie blue staining. The protein was stored in 20 mM Tris-HCl, pH 7.5, 100 mM NaCl, 1 mM dithiothreitol (DTT), and 5% glycerol at −80°C.

Dengue virus NS3 helicase protein expression and purification. The pDest17-H_6-NS3 plasmid was obtained from Bruno Canard's laboratory at AFMB, Universités d'Aix-Marseille, France (6), and the expression of His_6-NS3 protein was performed in *E. coli* BL21(DE3)/pDNAy and purified as follows. A 1-liter culture of *E. coli* BL21(DE3)/pDNAy/pDest17-NS3 containing 100 μg/ml ampicillin and 50 μg/ml kanamycin was grown to an optical density at 600 nm (OD_{600}) of 0.5 at 37°C. Two percent ethanol was added to the culture, which was then induced with 50 μM IPTG, chilled on ice for 2 h, and then incubated at 17°C overnight. Protein expression and purification were performed using Talon beads as described previously (61). The protein was eluted with 25 mM HEPES, pH 7.0, 0.5 M NaCl, 200 mM imidazole, and 0.1% Triton X-100. It was further purified on a Superdex 75 10/300GL column (20 mM Tris-HCl, pH 6.8, 200 mM NaCl, 1 mM DTT, and 5% glycerol). Fractions containing the desired protein were concentrated and stored at −80°C.

KF-mediated *E. coli* expression and purification. Cloning, expression, and purification were performed as described elsewhere (58). Briefly, Klenow fragment (KF) plasmid DNA (pET28-H_6-KF) was used to transform *E. coli* CJ376. An overnight inoculum of the expression strain was added to 500 ml LB broth at 30°C. At an A_{595} of 0.3, the incubation temperature was raised to 42°C to heat induce overproduction of the enzyme, and cells were grown for another 4 h. Cells were harvested, washed, and resuspended in cell lysis buffer (50 mM Tris-HCl, pH 8.0, 500 mM NaCl, 1 mM PMSF) containing 2 mg/ml lysozyme. Following sonication and centrifugation of the cell suspension (14,000 rpm for 30 min), the supernatant was passed through a DEAE column to remove DNA. The flowthrough was fractionated with ammonium sulfate, using 60 and 85% saturations. The pellet obtained with 85% ammonium sulfate was resuspended in 5 ml of buffer I (50 mM Tris-HCl, pH 7.0, 1 mM DTT, 1 mM EDTA), dialyzed overnight against 1 liter of the same buffer, and applied to a Bio-Rex 70 column prewashed with buffer I. The bound protein was eluted with a 50 to 500 mM linear gradient of NaCl in buffer I. Peak fractions (representing a 68-kDa protein on SDS-PAGE) were pooled, concentrated, buffer exchanged in 50 mM Tris-HCl, pH 7.0, 1 mM DTT, 100 mM NaCl, amended with 30% glycerol, and stored at −20°C.

Expression, purification, and gel-based primer extension assay of MoMLV RT and FMDV 3D pol. Expression, purification, and gel-based primer extension assays of Moloney murine leukemia virus reverse transcriptase (MoMLV RT) and foot-and-mouth disease virus 3D polymerase (FMDV 3D pol) were carried out as we have described previously (14, 44).

FRET-based screening assay using 96-well plates. The Maybridge Hitfinder chemical library of compounds was screened using a FRET-based assay. The chemical library was supplied as lyophilized films in 96-well plates. We used a Precision microplate pipetting system (BioTek, Winooski, VT) to suspend the compounds in 100% dimethyl sulfoxide (DMSO) to a final concentration of 10 mM (mother plates). From these plates, several sets of daughter plates, containing a 500 μM concentration of each compound (in 100% DMSO), were generated and stored at −80°C. Helicase reactions to generate fluorescence were carried out in a 96-well format. Specifically, each well contained 25 μl of a reaction mixture containing 20 mM HEPES, 20 mM NaCl, 0.01% bovine serum albumin (BSA), 2 mM DTT, 5% glycerol, 5 mM $MgCl_2$, 50 nM nsp13, and 20 μM inhibitor. The helicase reaction was initiated by the addition of 100 nM fluorescein- and black hole quencher-labeled dsDNA, 0.5 mM ATP, and a 2 μM concentration of unlabeled single-stranded DNA (ssDNA) with a sequence complementary to that of the BHQ-labeled DNA strand. The reactions were allowed to proceed for 10 min at 30°C. The change in fluorescence (excitation wavelength, 495 nm; emission wavelength, 520 nm) was measured immediately with a Quanta Master QM-1 T-format fluorescence spectrometer (Photon Technology International, Princeton, NJ).

Gel-based helicase assay. Helicase activity was measured by preincubating 50 nM nsp13 or 100 nM HCV NS3h or dengue virus NS3 with various concentrations of the inhibitor compound (0 μM, 2.5 μM, 5 μM, 10 μM, 20 μM, and 40 μM), followed by incubation with 100 nM forked substrate (dsRNA or dsDNA), 31/18-mer nucleic acid (13 single-stranded bases plus 18 double-stranded bases [13ss:18ds]) (dsDNA or dsRNA), or SARS-CoV-specific dsRNA (with the longer strand designed from nucleotides [nt] 7281 to 7311 of the SARS-CoV genome) (Fig. 1) in a reaction buffer containing 20 mM HEPES, pH 7.5, 20 mM NaCl, 1 mM DTT, 0.1 mg/ml BSA, 5 mM $MgCl_2$, and 2 mM ATP at 30°C for 10 min for nsp13 (20) or in a reaction buffer containing 20 mM MOPS (morpholinepropanesulfonic acid)-NaOH, pH 7.0, 5 mM magnesium acetate, 5 mM ATP, and 0.1 mg/ml BSA at 30°C for 30 min for NS3h (33). The reaction mixture also contained 2 μM unlabeled 18-mer DNA/RNA as a trap. Reactions were quenched by the addition of an equal volume of loading buffer (100 mM EDTA, 0.2% SDS, and 20% glycerol). Unless otherwise indicated, reactant concentrations refer to the final concentrations in the reaction mixture. The released ssDNA or RNA product and unwound dsDNA (or dsRNA) were resolved by 6% nondenaturing PAGE using a running buffer containing 89 mM Tris-borate, pH 8.2, and were run for 2 h at 4°C and 150 V. The control for measuring maximum unwinding was dsDNA denatured by heating for 5 min at 95°C and loaded immediately on the gel as suggested by Ahnert and Patel (2a). In this and subsequent assays, the gels were scanned with a phosphorimager (FLA 5000; FujiFilm). The band intensities representing ssDNA/ssRNA and dsDNA/dsRNA were quantitated using ImageQuant software (Pharmacia). The fraction of unwound DNA or RNA was plotted against the concentration of the compound (log), and the 50% effective concentration (EC_{50}) was determined by nonlinear regression using GraphPad Prism (GraphPad Inc.). Experiments were repeated at least three times.

ATP hydrolysis assay. ATP hydrolysis measurements were carried out under conditions similar to those used in the gel-based unwinding assays. nsp13 (50 nM) was preincubated with various concentrations of the inhibitor compound (0 μM, 2.5 μM, 5 μM, 10 μM, 20 μM, and 40 μM). Reactions were performed in a buffer consisting of 20 mM HEPES, pH 7.5, 20 mM NaCl, 5 mM $MgCl_2$, 1 mM DTT, 0.1 mg/ml BSA, and 5% glycerol and were initiated with 5 μM [γ-^{32}P]ATP. Samples were rapidly mixed at 30°C, and reactions were allowed to proceed for 10 s prior to quenching with 100 mM EDTA, 0.2% SDS, and 20% glycerol. Reaction products were separated by thin-layer chromatography on polyethyleneimine-cellulose F plates (Merck), using 0.5 M lithium chloride as the liquid phase, and were visualized by autoradiography. The fraction of hydrolyzed monophosphate (P_i) was quantitated using ImageQuant software (Pharmacia). Experiments were repeated at least three times.

DNA binding assay. To determine if the selected compound affected the binding affinity of nsp13 for nucleic acids, we performed gel mobility shift assays. We measured the binding of 60/40-mer (20ss:40ds) DNA substrates (Fig. 1) at various concentrations of the inhibitor in a reaction mixture containing 25 nM nsp13, 20 mM HEPES, pH 7.5, 20 mM NaCl, 5 mM $MgCl_2$, 1 mM DTT, 0.1 mg/ml BSA, and 5% glycerol at 30°C for 20 min. The concentration of 5′-Cy3-labeled dsDNA was 5 nM. Samples were electrophoresed at 100 V for 1.5 h at 4°C in a 6% nondenaturing polyacrylamide gel, using 89 mM Tris-borate, pH 8.2, as the buffer. Gels were scanned in a phosphorimager and quantitated by ImageQuant (Amersham Biosciences).

Enzyme kinetics. To determine the inhibition mode with respect to ATP (competitive or noncompetitive), we used a 96-well fluorescence-based assay to measure the effect of SSYA10-001 on the helicase activity of nsp13. Twenty-five-microliter reaction mixtures containing 50 nM nsp13, 20 mM HEPES, pH 7.5, 20 mM NaCl, 5 mM $MgCl_2$, and various SSYA10-001 concentrations (0 to 20 μM) were initiated by adding 100

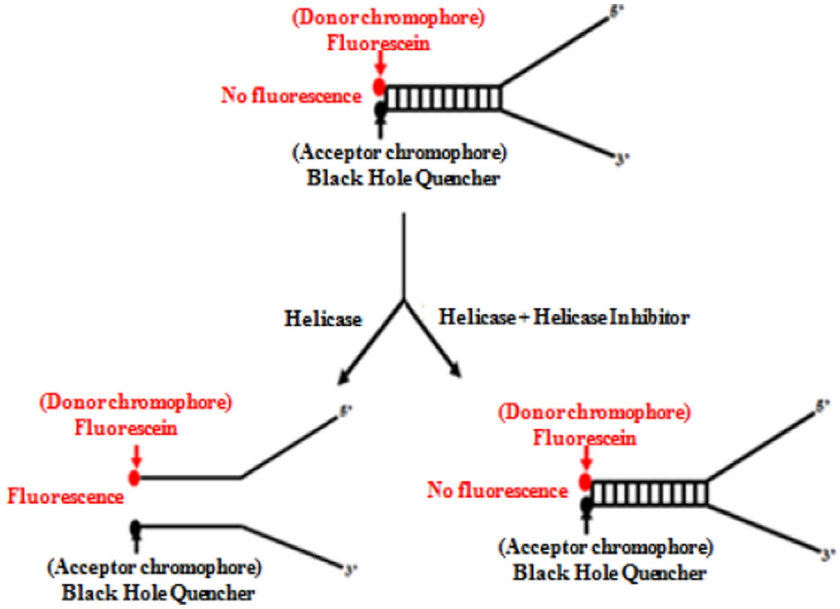

FIG 2 Schematic representation of the fluorescence helicase assay. A dsDNA substrate (forked substrate) was designed with 2 chromophores at the ends of the complementary strands (i.e., fluorescein and black hole quencher). In the presence of an active helicase, the two complementary strands are separated, allowing fluorescence detection of the fluorescein chromophore, whose excitation occurs at 495 nm and emission occurs at 520 nm. In the presence of a potential helicase inhibitor, the two complementary strands will not be separated; therefore, fluorescence will not be detected.

nM fluorescein- and black hole quencher-labeled dsDNA. These reaction mixtures also included increasing amounts of ATP (0.0125 mM to 7.5 mM). To determine the inhibition mode with respect to nucleic acids, the fluorescein- and black hole quencher-labeled substrate concentrations were varied (0.01 μM to 1 μM) in the presence of 2 mM ATP and increasing amounts of SSYA10-001 (from 0 to 20 μM). The reactions were allowed to proceed for 10 min at 30°C, and fluorescence was measured as described above. Assays were carried out in three independent experiments. Results were analyzed in Lineweaver-Burk graphs ($1/V$ versus $1/[S]$ for various SSYA10-001 concentrations), and Dixon plots ($1/V$ versus [SSYA10-001]) were used to determine the inhibitor K_i from the x axis intercept (53) (GraphPad Prism 5.0; GraphPad Inc.).

Primer extension and strand displacement assay with Klenow fragment. The DNA template was annealed to a 5′-Cy3-labeled DNA primer and a third oligonucleotide, corresponding to the first 14 nucleotides of the DNA template at the 5′ end (Fig. 1; see Fig. 8). To monitor primer extension, a 10 nM concentration of DNA substrate (14ds:4ss:18ds DNA substrate) (Fig. 1) was incubated with various concentrations of SSYA10-001 (0, 5, 10, and 20 μM) or Pico green reagent (Invitrogen) (0×, 1×, 2×, and 3×, as directed by the manufacturer) in a buffer containing 50 mM Tris, pH 7.5, 50 mM NaCl, 5 mM $MgCl_2$, 1 mM DTT, and 5% glycerol. The reactions were initiated by the addition of 20 nM KF to a final volume of 20 μl. All deoxynucleoside triphosphates (dNTPs) were present at a final concentration of 50 μM. The reactions were terminated after 15 min by adding an equal volume of 100% formamide containing traces of bromophenol blue. The products were resolved in a 15% polyacrylamide-7 M urea gel. In this and subsequent assays, the gels were scanned with a phosphorimaging device (FLA 5000; FujiFilm).

Pico green assay. To measure Pico green activity, a 1× final concentration of Pico green reagent was incubated with 50 nM dsDNA (31/18-mer) in a buffer containing 10 mM Tris-HCl, 1 mM EDTA, pH 7.5, in a total volume of 200 μl in a 96-well microplate, and fluorescence was measured ~2 min after the start of incubation, using a CytoFluor microplate reader. Samples were excited at 485 nm, and fluorescence intensity was measured at 520 nm. To determine if SSYA10-001 binds nucleic acids, various concentrations of the compound (0, 2.5, 5, 10, 20, and 40 μM) were preincubated with 50 nM dsDNA (31/18-mer) for 10 min, followed by addition of a 1× final concentration of Pico green reagent and immediate fluorescence measurement.

SARS-CoV replicon assay with RNA detection by RT-qPCR. The SARS-CoV replicon was prepared as described previously (4). A Rep1b deletion mutant (most of the Rep1b region has been deleted) was generated by digesting and ligating the SARS-CoV replicon with Bsu361 at regions 16562 to 16565 and 29013 to 29016 of the SARS-CoV replicon. 293T cells were grown to 95% confluence in 35-mm-diameter plates and transfected with 4 μg of SARS-CoV replicon, the SARS-CoV nonreplicative construct (NRC) (Rep1b deletion mutant), or mock plasmid by use of Lipofectamine reagent (Invitrogen) as directed by the manufacturer. Various concentrations of SSYA10-001 (0, 2.5, 5, 10, and 20 μM) were added to the replicon-transfected cells and NRC-transfected cells. Total intracellular RNA was extracted at 48 h posttransfection (hpt), using TRIzol reagent (Invitrogen) followed by DNase I treatment to digest any remnant DNA. The extracted RNA was used as a template for reverse transcription-quantitative real-time PCR (RT-qPCR) analysis of N gene mRNA synthesis (NC). The reverse primer URB-28630RS (5′-TGCTTCCCTCTGCGT AGAAGCC-3′), complementary to nucleotides 511 to 532 of the N gene, and the forward primer URB-29VS (5′-GCCAACCAACCTCGATCTCT TG-3′), spanning nucleotides 29 to 50 of the Urbani leader sequence, were used for amplification using a SuperScript One-Step RT-qPCR system with Platinum *Taq* DNA polymerase (Invitrogen), adhering to the manufacturer's specifications. This system is a real-time quantitative PCR system that utilizes Sybr green for detection and quantitation of the amplified DNA. The sequences for the forward and reverse primers for the amplification of U6 mRNA as an endogenous control were as follows: 5′CTCGCT TCGGCAGCACA-3′ for the U6 forward primer and 5′-AACGCTTCAC GAATTTGCGT-3′ for the U6 reverse primer. Primer pair amplification efficiencies were determined using 1:10 cDNA dilutions; test and housekeeping gene primer pairs with similar efficiencies were used for the qPCRs. Samples were normalized internally by using the cycle threshold (C_T) of the housekeeping gene U6 as follows: $\Delta C_T = (C_T \text{NC}) - (C_T \text{U6})$. This was followed by determination of the mean for each sample, since the reactions were performed in triplicate. The mean value for each sample was normalized to the mean value for the NRC-transfected cells by use of the following equation: $\Delta\Delta C_T = \Delta C_T(\text{sample}) - \Delta C_T(\text{NRC})$. Relative

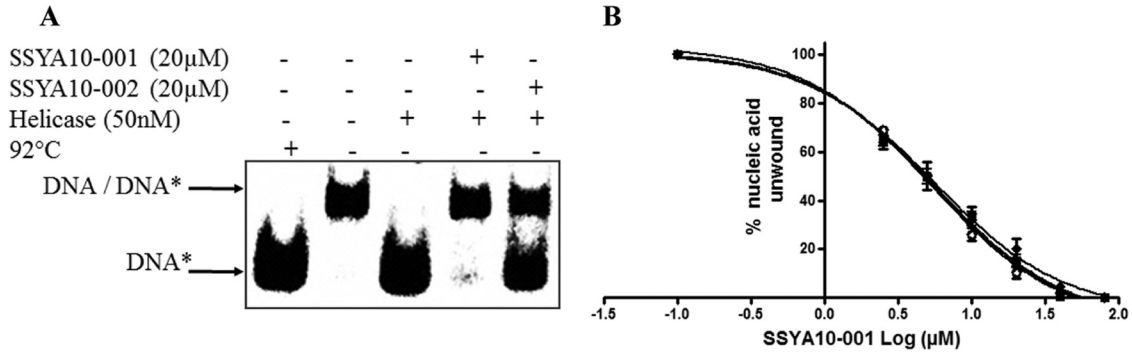

FIG 3 Validation of nsp13 inhibition by use of a gel-based helicase assay. (A) nsp13 (50 nM) was incubated in the presence of 20 μM inhibitor compound, 20 mM HEPES, 20 mM NaCl, 0.01% BSA, 2 mM DTT, 5% glycerol, and 5 mM $MgCl_2$. The helicase reaction was initiated by the addition of 100 nM 31/18-mer (13ss:18ds) as the substrate (Cy3 labeled) at 30°C, along with 0.5 mM ATP and a 2 μM concentration of unlabeled ssDNA with a sequence complementary to that of the unlabeled DNA strand. The reactions were allowed to proceed for 10 min at 30°C, and the reaction was quenched with 100 mM EDTA, 0.2% SDS, and 20% glycerol. The products were separated and analyzed by 6% nondenaturing PAGE. (B) The IC_{50} of SSYA10-001 was determined using the gel-based assay described for panel A with various concentrations of the compound (0, 2.5, 10, 20, 40, and 80 μM). Reaction products were resolved and quantitated using ImageQuant software (Pharmacia). The fractions of unwound DNA (○), RNA (■), and SARS-CoV-specific RNA (◆) were plotted against the concentrations of inhibitor, and the data were fit to dose-response curves by use of GraphPad Prism 5.0 (GraphPad Inc.) to determine the IC_{50} (mean ± standard deviation [SD]): 5.7 ± 2.3 μM with 31/18-mer RNA (13ss:18ds), 5.6 ± 0.5 μM with SARS-CoV-specific 31/18-mer RNA (13ss:18ds), and 5.3 ± 2.0 μM with 31/18-mer DNA (13ss:18ds). Experiments were performed three times, and error bars represent standard deviations for the three independent experiments.

quantity (RQ) values were calculated as follows: $RQ = 2^{-\Delta\Delta CT}$. The RQ value for each sample was then normalized to the RQ value for the NRC (which is 1) in order to obtain percent relative RQ values. The data were graphed as percent relative replicon activities against the log values of the inhibitor concentrations (in μM), using a dose-response curve in GraphPad Prism 5.0 (GraphPad Inc.). Data presented represent 3 independent experiments performed in triplicate.

RNA detection by RPA. Total RNA was obtained as described above. The RNase protection probes were generated by cloning SARS-CoV fragments from nt 7281 to 7431 (total of 150 nt) into the EcoRI and XbaI restriction sites of the T7/Sp6-driven pGEM-3Z transcription vector (Promega), followed by transcript generation through Sp6-controlled *in vitro* transcription with NTPs and radioactive UTP incorporation to obtain an antisense probe (43, 54). The antisense probe generated was 182 nt long because of the extra 32 nt between the Sp6 transcription start site and the XbaI site of the pGEM-3Z vector. This was followed by DNase I treatment and RNA isolation using a phenol-chloroform RNA extraction protocol. RNase protection assays (RPAs) were performed at 55°C by overnight annealing of the newly generated probes with each of the total intracellular RNA samples containing different concentrations of SSYA10-001. This was followed by RNase A and T1 treatment of the annealed reaction mixtures. The reaction samples were analyzed in a 6% urea-polyacrylamide gel and visualized using a phosphorimager (FLA 5000; FujiFilm).

Assessment of cytotoxicity. We assessed the effects of the inhibitor on cellular viability by using a commercially available kit (Roche Diagnostics, Indianapolis, IN) that measures metabolism of XTT {2,3-bis(2-methoxy-4-nitro-5-sulfophenyl)-5-[(phenylamino)carbonyl]-2H-tetrazolium hydroxide}. XTT is a tetrazolium salt that is converted by mitochondrial succinate dehydrogenase to a soluble orange-colored formazan product which retains activity only in metabolically active cells. The amount of product is proportional to the number of living cells and can be quantified spectrophotometrically. The assay was performed in triplicate as described previously (14). Briefly, human embryonic kidney (HEK 293T) cells were seeded to 90% confluence in a 96-well plate. Cells were incubated for 48 h with various concentrations of inhibitor (50 nM to 250 μM) in a final volume of 100 μl Dulbecco's modified Eagle's medium (DMEM) with 10% fetal bovine serum (FBS) and 50 μg/ml penicillin G and streptomycin. Cells treated with Triton X-100 were used as a control for loss of cell viability. After the 48-hour incubation period, the medium was removed and replaced with phenol red-free medium. Twenty microliters of XTT was added per well, and cells were incubated for an additional 3.5 h. After incubation, the optical density at 450 nm was read by a plate reader, and the 50% cytotoxic concentration (CC_{50}) was determined by plotting the percent relative cell viability against the inhibitor concentration, using a sigmoidal dose-response curve in Graphpad Prism 5.0 (GraphPad Inc.).

Cell cytostatic assay. To assess the cytostatic effect of the compound, 7.5×10^5 cells/well of HEK 293T cells were seeded in 6-well plates, and the cells were maintained in a final volume of 2 ml DMEM with 10% FBS and 50 μg/ml penicillin G and streptomycin. SSYA10-001 (250 μM) was added to each well, and the medium was changed daily, with fresh compound added each time. The cells were collected at 0, 12, 24, and 48 h, and viability was determined by the trypan blue exclusion method and counted on a hemocytometer (49). To perform the trypan blue exclusion method, cell samples were diluted 1:1 in a 0.4% trypan blue solution. Blue cells were regarded as nonviable, while the viable cells were unstained. The

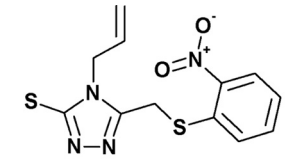

SSYA10-001 (IC50=6 μM)
3-[(2-nitrophenyl)sulfanylmethyl]-4-prop-2-enyl-1H-1,2,4-triazole-5-thione

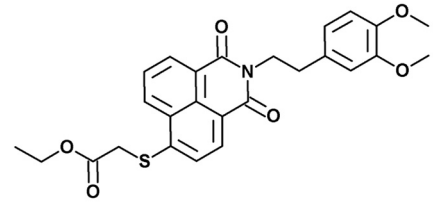

SSYA10-002 (IC50=20 μM)
ethyl 2-[2-[2-(3,4-dimethoxyphenyl)ethyl]-1,3-dioxobenzo[de]isoquinolin-6-yl]sulfanylacetate

FIG 4 Chemical structures, names, and IC_{50}s of the identified nsp13 inhibitors.

TABLE 1 Concentration parameters of SSYA10-001[a]

Parameter	Value (μM)
IC_{50}	
RNA	5.7 ± 0.74
DNA	5.3 ± 0.40
SARS-CoV RNA	5.6 ± 0.50
EC_{50} for SARS-CoV replicon (in RT-qPCR)	8.95 ± 0.86
CC_{50}	>250

[a] IC_{50}s were determined from the helicase gel-based assay, and EC_{50} and CC_{50} values were determined from the replicon cell-based assay. All values were obtained by using a dose-response curve in GraphPad Prism 5.0 (GraphPad Inc.). Experiments were performed three times, and the values represent means ± standard deviations.

number of viable cells counted was plotted against time, using GraphPad Prism 5.0 (GraphPad Inc.). Experiments were performed in triplicate.

RESULTS

FRET-based helicase assay in 96-well plates. To monitor the unwinding activity of nsp13, we used a fluorescence assay that utilizes a dsDNA substrate with two chromophores (fluorescein donor and black hole quencher acceptor) placed on opposite strands but near each other, on the 5′ and 3′ ends of the opposing strands (Fig. 2). An active helicase will separate the two strands, and a fluorescence signal will be observed as a result of photon emission from the fluorescein chromophore (6-carboxyfluorescein [FAM]). No fluorescence will be observed if there is no strand separation because the emitted photons from the fluorescein will be absorbed by the black hole quencher, thereby preventing the detection of fluorescein signals. The sequence of the reaction is shown in Fig. 2. Fluorescence signals were detected at 520 nm (with excitation at 495 nm). To assess the quality of this assay, we determined the *z* factor to be 0.66 under our experimental conditions. This value suggests that this is an excellent assay, as described by Zhang et al. (72).

Chemical library screening. Using the assay described above, ~3,000 compounds were screened from the Maybridge HitFinder chemical library, and we selected only two compounds (SSYA10-001 and SSYA10-002) that suppressed fluorescence by >50%. The positive hits may include compounds that affect the fluorescence of fluorescein and, as a consequence, are false-positive hits. Therefore, to rule out such false-positive results, we validated the compounds' ability to specifically inhibit nsp13's unwinding activity in a gel-based assay that utilizes fluorescently labeled nucleic acids. We found that SSYA10-001 inhibited the nucleic acid unwinding activity of nsp13 (Fig. 3), with almost 100% inhibition of the helicase activity at 20 μM SSYA10-001. SSYA10-002 was considerably less potent. Hence, SSYA10-001 was characterized further with respect to nsp13's unwinding activity. The chemical structures and names of the compounds are shown in Fig. 4.

Effect of SSYA10-001 on nsp13's unwinding activity on dsRNA substrate. We recently showed that nsp13 can unwind dsRNA and dsDNA equally well (2). Since RNA is the biological substrate of nsp13, we monitored the effect of SSYA10-001 on nsp13's unwinding activity on dsRNA (31/18-mer) and SARS-CoV-specific dsRNA. As shown in Fig. 3B and Table 1, SSYA10-001 had similar IC_{50}s for the inhibition of nsp13's unwinding activity on dsRNA (31/18-mer), dsDNA (31/18-mer), and SARS-CoV-specific dsRNA (IC_{50}s of 5.70, 5.30, and 5.60 μM, respectively).

SSYA10-001 specifically inhibits SARS-CoV helicase. To determine if SSYA10-001 is specific for nsp13 inhibition, we monitored and compared the effects of SSYA10-001 on the SARS-CoV nsp13, HCV NS3h, and dengue virus NS3 helicases. The result in Fig. 5A shows that SSYA10-001 inhibition of helicase activity is specific for the SARS-CoV helicase. Moreover, SSYA10-001 did not cause inhibition of RNA and DNA polymerases, including FMDV 3D pol, MoMLV reverse transcriptase, or KF (Fig. 5B).

Kinetic mechanism of inhibition. To establish the mode of inhibition of nsp13 by SSYA10-001, we determined the kinetic mechanism of inhibition and the K_i value. The Lineweaver-Burk plots in Fig. 6A and B each comprise a series of five lines (one for each inhibitor concentration) intersecting at the same point on the *x* axis ($-1/K_m$), which is a hallmark of noncompetitive inhibition (8, 51). Hence, nsp13 inhibition by SSYA10-001 is noncompetitive with respect to both ATP and the nucleic acid substrate. The K_i value for SSYA10-001 obtained from the Dixon plot ($1/V$ versus [SSYA10-001] [data not shown]) was 6.0 ± 1.7 μM.

SSYA10-001 does not prevent DNA binding and ATP hydrolysis by SARS-CoV nsp13. To determine whether SSYA10-001 inhibits the unwinding activity of nsp13 by interfering with nsp13's nucleic acid binding capability, we monitored the DNA binding of nsp13 in the presence and absence of various concentrations of SSYA10-001 and analyzed the reaction by using a gel shift mobility assay. As shown in Fig. 7A, SSYA10-001 did not

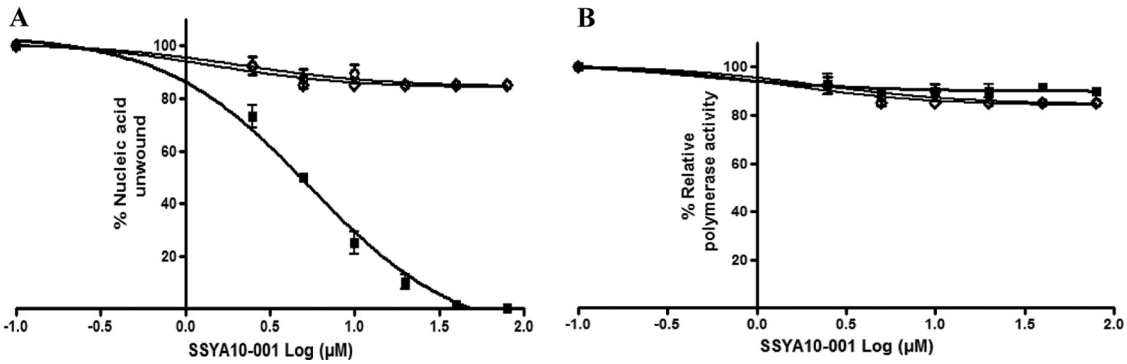

FIG 5 Effect of SSYA10-001 on activity of other helicases and polymerases. (A) Plot of the fractions of unwound RNA for the HCV NS3h helicase (◇), dengue virus NS3 helicase (○), and SARS-CoV nsp13 helicase (■). Experiments were performed three times, and error bars represent standard deviations for three independent experiments. (B) Plot of the fractions of polymerization product for KF (◇), MoMLV RT (○), and FMDV 3D pol (■). Experiments were performed three times, and error bars represent standard deviations for three independent experiments.

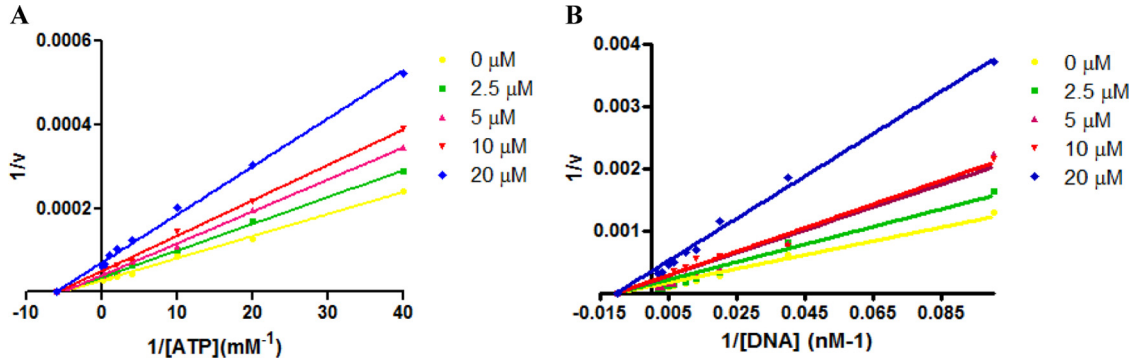

FIG 6 Noncompetitive inhibition of nsp13 by SSYA10-001 under steady-state conditions. Kinetic experiments with nsp13 were conducted in 96-well plates by using a fluorescence-based assay (see Materials and Methods) in the presence of increasing concentrations of SSYA10-001 (0 to 20 μM), varying either the ATP substrate (0.0125 mM to 7.5 mM) (A) or the forked substrate (0.01 μM to 1 μM) (B). In both cases, the *x* axis intercept ($-1/K_m$ for the ATP or forked substrate) was not affected by the inhibitor concentration, and this is a feature of noncompetitive inhibition.

affect the ability of nsp13 to bind DNA. Similarly, we assessed the ATP hydrolysis of nsp13 with an increase in the concentration of SSYA10-001; the result shows that hydrolysis of ATP by nsp13 is not inhibited by SSYA10-001 (Fig. 7B).

SSYA10-001 does not chelate double-stranded nucleic acids. To rule out the possibility of SSYA10-001 binding the nucleic acid substrate, we performed a gel-based primer extension-strand displacement assay. We designed a blocker substrate as shown in Fig. 8A, with a 14-nt complementary strand acting as a blocker at the 5′ end of the template strand. We then performed a primer extension assay with and without SSYA10-001 and with the Klenow fragment of *E. coli* DNA polymerase I (KF) (59), which has both polymerase and strand displacement activities. The results in Fig. 8B demonstrate that SSYA10-001 does not prevent KF from performing its polymerization and strand displacement activities, suggesting that SSYA10-001 does not bind nucleic acids. To validate this assay, we conducted the same experiment as that described above, except that SSYA10-001 was replaced with Pico green, a known nucleic acid chelator, as a positive control. The result in Fig. 8C shows that Pico green interferes with the ability of KF to extend the primer and displace the blocker from the strand because of Pico green's DNA-chelating (minor groove-binding) ability. To further evaluate the possibility of SSYA10-001 binding to DNA, various concentrations of SSYA10-001 (0, 2.5, 5, 10, 20, and 40 μM) were preincubated with dsDNA (31/18-mer) for 10 min, followed by addition of a 1× final concentration of Pico green reagent and immediate fluorescence measurement. The fluorescence counts from Pico green interaction with the dsDNA did not change with increasing concentrations of SSYA10-001, suggesting that SSYA10-001 does not bind DNA (Fig. 8D).

Inhibition of SARS-CoV replication by SSYA10-001. To monitor the effect of SSYA10-001 on the replication of SARS-CoV, we performed a SARS-CoV replicon assay as described in Materials and Methods. The SARS-CoV replicon and the NRC were cloned into a pBAC plasmid which contained a cytomegalovirus (CMV) promoter. To eliminate the possibility of SSYA10-001 inhibiting RNA polymerase II (RNA Pol II) or the CMV promoter, various concentrations of SSYA10-001 were added to the NRC-transfected cells; no difference was observed between the amounts of RNA synthesized in the presence and absence of SSYA10-001 in the NRC-transfected cells (data not shown). Hence, the amount of DNA amplicon measured from the nonreplicative construct was regarded as the background, and as a result, the amount of DNA amplified from the SARS-CoV replicon was normalized with the quantified DNA amplicon from the nonreplicative construct after normalization of all samples to the C_T counts of the housekeeping gene, U6, as a control. The average raw C_T count for the SARS-CoV replicon without compound was ~21, compared to an average of ~28 for the NRC before normalization to the C_T count of U6 (~18). Following normalization to U6, with additional normalization to NRC and using the $2^{-\Delta\Delta CT}$ value to obtain the RQ, the amount of DNA amplified from the SARS-CoV replicon was ~100-fold in excess over the amount of DNA amplicon amplified from the NRC. We performed these

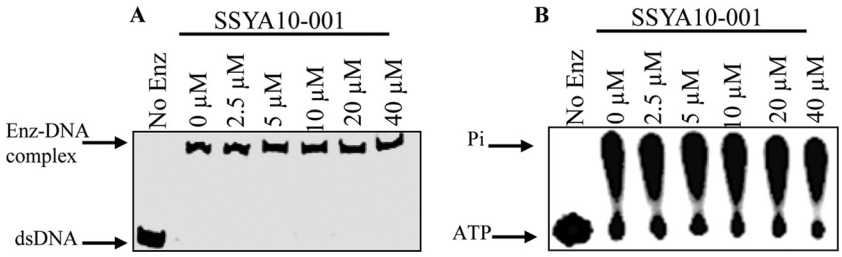

FIG 7 Investigation of the effect of SSYA10-001 on nucleic acid binding and ATP hydrolysis of nsp13. (A) nsp13 (25 nM) was preincubated with various concentrations of SSYA10-001 (0, 2.5, 10, 20, and 40 μM) followed by incubation with a 5 nM concentration of a Cy3-labeled version of the forked substrate in 20 mM HEPES (pH 7.5), 20 mM NaCl, 5 mM $MgCl_2$, 1 mM DTT, 0.1 mg/ml BSA, and 5% glycerol at 30°C for 20 min. The reaction samples were then analyzed in a nondenaturing 6% polyacrylamide gel. (B) Preincubated nsp13 (50 nM) and various concentrations of SSYA10-001 (0, 2.5, 10, 20, and 40 μM) were mixed with 5 μM [γ-^{32}P]ATP for 10 s. The reaction products were separated by thin-layer chromatography and visualized by autoradiography.

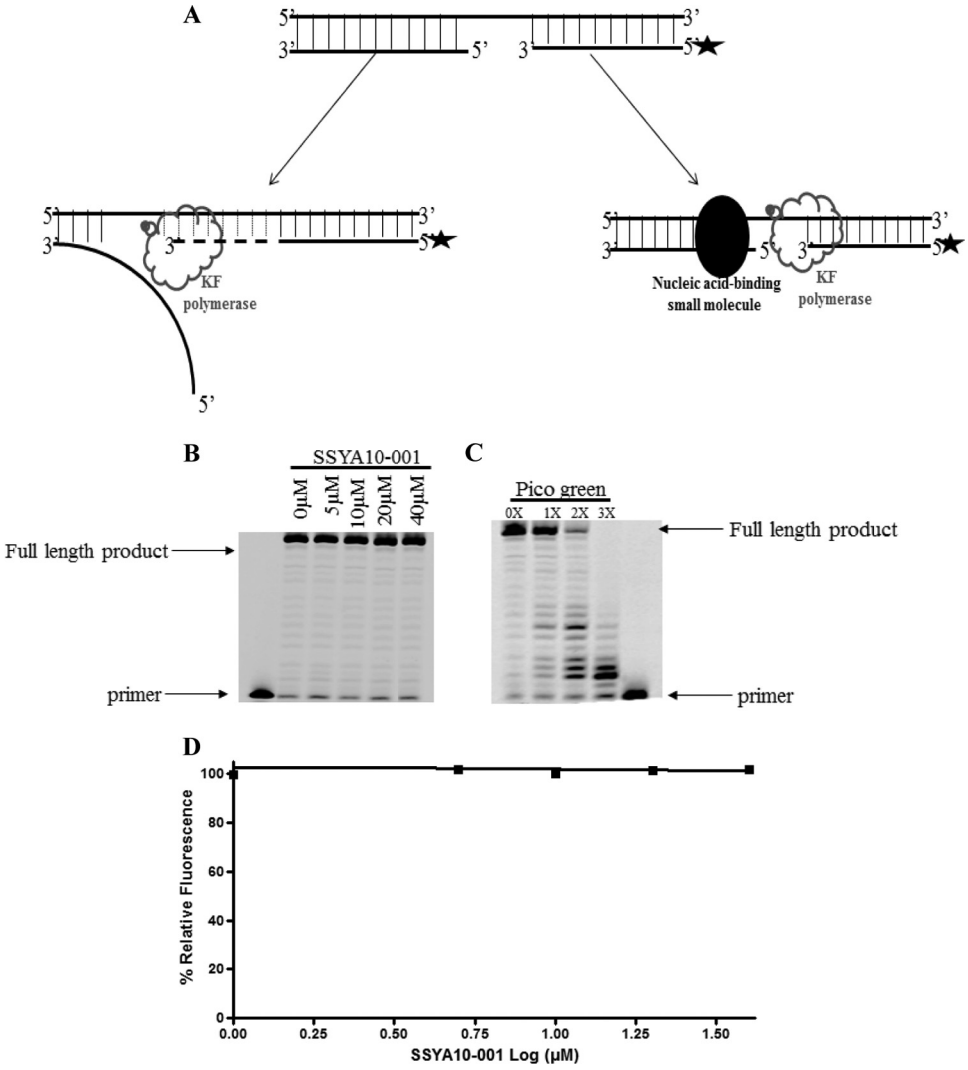

FIG 8 Determination of nucleic acid binding of SSYA10-001. (A) Klenow fragment strand displacement and polymerization assay design. A DNA substrate with a 3′-end primer is annealed with a complementary strand at the 5′ end. Primer extension can take place only in the presence of a polymerase with strand displacement activity, such as KF. The presence of a dsDNA chelator such as Pico green will prevent strand displacement and therefore prevent primer extension. (B and C) Various concentrations of SSYA10-001 (0, 5, 10, and 20 μM) (B) and Pico green (1×, 2×, and 3×) (C) were preincubated with 20 nM 13ds:4ss:18ds DNA substrate in a mixture including 50 mM Tris-HCl, pH 7.5, 50 mM NaCl, 5 mM $MgCl_2$, 1 mM DTT, 5% glycerol, and a 50 μM concentration of each dNTP. The reaction was initiated by the addition of 20 nM KF at 37°C for 10 min, and the reactions were resolved and analyzed in a 15% polyacrylamide-7 M urea gel. (D) Various concentrations of SSYA10-001 (0, 2.5, 5, 10, 20, and 40 μM) were preincubated with dsDNA (31/18-mer) for 10 min, followed by addition of a 1× final concentration of Pico green reagent and immediate fluorescence measurement. The percent relative fluorescence was plotted against the concentration of the inhibitor, and the data were fit to dose-response curves by use of GraphPad Prism 5.0 (GraphPad Inc.). Experiments were performed in triplicate in two independent experiments.

experiments with the SARS-CoV replicon in the presence and absence of various concentrations of SSYA10-001, and as shown in Fig. 9A and Table 1, SSYA10-001 inhibited SARS-CoV replication, with an EC_{50} of 8.95 μM. To confirm this result, we performed RPAs as described in Materials and Methods to further monitor the amount of RNA synthesized in the presence of various concentrations of SSYA10-001. As shown in Fig. 9B, SSYA10-001 interfered with SARS-CoV replication.

Evaluation of cytotoxicity. SSYA10-001 was evaluated for its effect on cell viability in the XTT cell viability assay. HEK 293T cells were incubated with various concentrations of SSYA10-001 for 48 h. No cytotoxicity was observed for SSYA10-001 at 250 μM (Table 1). We therefore estimated that the CC_{50} of SSYA10-001 is >250 μM. To investigate the cytostatic effect of SSYA10-001, we conducted a cell cytostatic assay as described in Materials and Methods, and as shown in Fig. 10, SSYA10-001 did not interfere with the proliferation of HEK 293T cells.

DISCUSSION

Helicases are motor proteins that unwind double-stranded nucleic acids into two single-stranded nucleic acids by utilizing the energy derived from nucleotide hydrolysis. Helicases may unwind dsDNA and/or dsRNA substrates and may be active as monomers or multimers (6, 36–38, 42, 47, 48); they may also be involved in protein-protein interactions (69) and interactions with host factors (10). Hence, they are valid antiviral targets that have yet to be

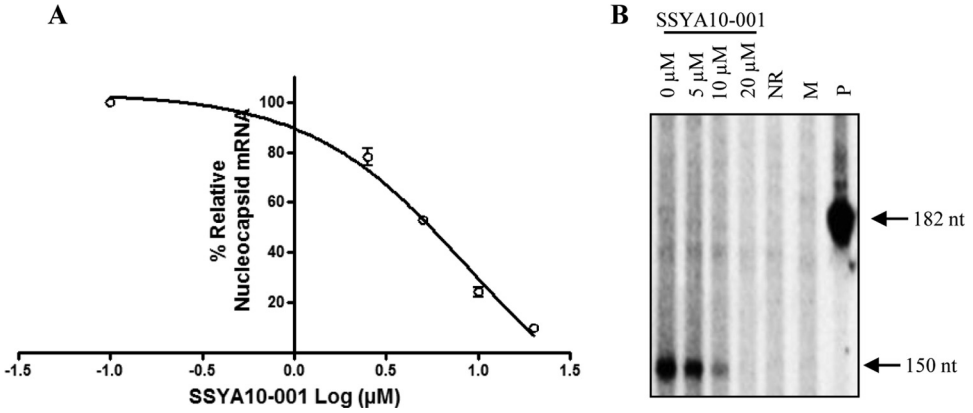

FIG 9 Measurement of SARS-CoV replication in the presence of SSYA10-001. (A) HEK 293T cells were mock transfected or transfected with the SARS-CoV replicon or a nonreplicative construct by use of Lipofectamine 2000 (Invitrogen) in the presence of various concentrations of SSYA10-001 (0, 2.5, 5, 10, and 20 μM). Total RNA was isolated at 48 h posttransfection and analyzed by RT-qPCR with specific oligonucleotides to detect N gene mRNA. Triplicate RT-qPCR products were amplified in parallel. The average N gene mRNA quantity for each concentration was normalized internally by using the C_T of the housekeeping gene U6. Samples were additionally normalized to the NRC controls, and the RQ value for each sample was obtained using the relative quantity method ($2^{-\Delta\Delta CT}$). The RQ value for each sample was then normalized to the RQ value of the NRC (which is 1), and the data were graphed as percent relative replicon activities against the log inhibitor concentrations (in μM) by use of a dose-response curve in GraphPad Prism 5.0 (GraphPad Inc.). Experiments were repeated three times, and error bars represent standard deviations for triplicate samples. (B) HEK 293T cells were mock transfected or transfected with the SARS-CoV replicon or a nonreplicative construct by use of Lipofectamine 2000 (Invitrogen) in the presence of various concentrations of SSYA10-001 (0, 5, 10, and 20 μM). Total RNA was isolated at 48 h posttransfection. An RNase protection assay was performed by overnight annealing of the newly generated probes with the total intracellular RNA, followed by RNase A and T1 treatment of the annealed reaction mixture. The reaction samples were analyzed in a 6% urea-polyacrylamide gel and visualized using a phosphorimager (FLA 5000; FujiFilm). Lanes: P, the probe by itself; MT, mock transfection; NR, sample from the nonreplicative construct. The probe was 182 nt long because of the extra 32 nt between the Sp6 transcription start site and the XbaI site of the pGEM-3Z vector.

explored, in part because some inhibitors of helicases may also be competitive inhibitors at the ATP binding site or bind nonspecifically at the nucleic acid binding cleft of other host cellular proteins, such as cellular kinases, which are required for normal cellular metabolism.

Although helicases act as molecular engines that unwind nucleic acids during replication, recombination, and DNA repair (19), recent reports have shown that they could also be required for other biological processes, such as displacement of proteins from nucleic acids, movement of Holliday junctions, chromatin remodeling, catalysis of nucleic acid conformational changes (11, 17, 21, 32, 67, 68), several aspects of RNA metabolism (including transcription, mRNA splicing, mRNA export, translation, RNA stability, and mitochondrial gene expression [66]), and viral replication (13, 56, 65). As a result, they are potential targets for treatment of diseases, including neoplastic diseases and viral infections (24, 30, 57). Nonetheless, to our knowledge, there are currently no approved drugs that target any viral, bacterial, or host helicase.

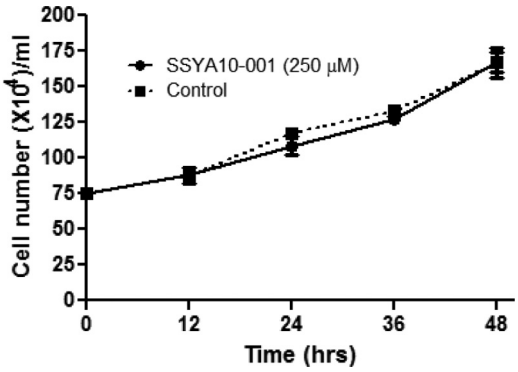

FIG 10 Cytostatic effect of SSYA10-001. HEK 293T cells (7.5×10^5) were treated with 250 μM SSYA10-001. The medium was changed and fresh compound added daily. Viability of the cells was assessed every 12 h through 48 h by trypan blue exclusion. The number of viable cells counted was plotted against time, using Graphpad Prism 5.0 (GraphPad Inc.). Experiments were performed in triplicate, and error bars represent standard deviations for triplicate samples. ●, 250 μM SSYA10-001; ■, 0.2% DMSO control.

Other studies have previously identified potential inhibitors of the SARS-CoV helicase, nsp13 (23, 31, 62, 71). Some of these inhibitors have not been evaluated in cell-based studies, and their effects on the dsRNA unwinding activity of nsp13 have yet to be determined. In addition, the mechanism of action for most of these compounds is unknown. Ideally, a compound that targets a viral helicase should block viral replication without affecting cellular functions. For example, compounds that prevent nucleic acid binding are likely to interfere with the functions of related cellular enzymes and would not be suitable for therapeutic purposes. In addition, compounds that might interfere with binding and/or hydrolysis of ATP may also interfere with the ATPase activity of other cellular ATPases or kinases and cause adverse side effects. In that respect, previously reported nsp13 inhibitors shown to interfere with both unwinding and ATPase activities of nsp13 are likely to impede normal cellular activities.

In this study, we used a FRET-based screening assay for the identification of SARS-CoV helicase inhibitors in the Maybridge Hitfinder chemical library of compounds. This chemical library contains ~14,000 compounds that follow Lipinski's rule of five, an empirical rule that is used to evaluate "drug-likeness" and potential for oral bioavailability in humans (35). This assay utilized a preliminary screening concentration of 20 μM, and the preliminary candidate compounds were selected based on their ability to

reduce fluorescence activity by more than 50%. The preliminary candidates were validated with the traditional "all-or-none" gel-based helicase assay (Fig. 2), which directly monitors the final product of the reaction (ssDNA or ssRNA) (3, 15, 18, 34, 39). Two compounds were found to inhibit SARS-CoV helicase activity. However, only one (SSYA10-001) was selected for further characterization due to its potency.

Activity of SSYA10-001 against SARS-CoV replication was confirmed by demonstrating that SSYA10-001 reduced the levels of SARS-CoV RNA in replicon-transfected cells, with an EC_{50} of ~9 μM (Fig. 9 and Table 1). Further cytotoxicity measurements indicated that the CC_{50} for SSYA10-001 was >250 μM. Since the antiviral activity of the compound is ~9 μM, the selectivity index (CC_{50}/EC_{50}) is ~30. Currently, we are assessing analogs of this original compound to identify compounds with improved antiviral properties. SSYA10-001 is a derivative of the triazole group. Some derivatives of triazole consist of compounds that have been shown to have high bioavailability (55), with some of them demonstrating anti-inflammatory, antimycobacterial, antimicrobial, anticonvulsant, and analgesic activities (1, 9, 22, 26, 27, 29). Interestingly, a triazole-3-thione compound which is closely related to SSYA10-001 was shown to be a potent antithyroid compound with low toxicity (28). All of these properties of closely related compounds of SSYA10-001 suggest that this compound may be a promising druggable lead that can be an effective antiviral agent that could potentially exhibit good pharmacokinetics.

To determine the specificity of SSYA10-001 and to eliminate the possibility that it promiscuously binds other nucleic acid binding proteins, we assessed its effects on the enzymatic activities of several viral or bacterial polymerases and helicases. These included two other viral helicases (HCV NS3 and dengue virus NS3), a retroviral reverse transcriptase (MoMLV RT), a viral RNA polymerase (FMDV 3D pol), and a bacterial DNA polymerase. Our results demonstrate that SSYA10-001 is specific for SARS-CoV helicase inhibition (Fig. 5). Hence, SSYA10-001 does not bind nonspecifically to dNTP or NTP binding pockets of polymerases, NTP binding pockets of helicases, or nucleic acid binding domains of polymerases or helicases. These results are consistent with our kinetic studies demonstrating that SSYA10-001 does not competitively inhibit the binding of nucleic acids and ATP to nsp13 (Fig. 6A and B).

Since our results show that SSYA10-001 does not inhibit nsp13's binding and hydrolysis of nucleic acids and ATP, coupled with the fact that SSYA10-001 does not bind the nucleic acid substrate, it is likely that SSYA10-001 inhibits unwinding by affecting conformational changes during the course of the reaction or translocation on the nucleic acid.

Given the high homology between SARS-CoV helicase and other coronavirus helicases (~70%) (data not shown), SSYA10-001 may also inhibit several coronaviruses that cause human disease, including but not limited to HCoV-229E and NL63. Further studies are under way to evaluate these predictions.

In conclusion, we have identified small-molecule inhibitors of SARS-CoV replication that block the helicase activity of nsp13. SSYA10-001 will be used to study the role of helicases in coronavirus replication, which could be a model for other nidoviruses. It may also serve as a lead for the development of antivirals for the treatment of SARS-CoV infections.

ACKNOWLEDGMENTS

This work was supported in part by NIH grants AI076119, AI094715, AI079801, and AI074389. We also acknowledge support by a grant from the Ministry of Knowledge and Economy, Bilateral International Collaborative R&D Program, Republic of Korea.

We are grateful to Charles Rice for providing the plasmid for expression of HCV NS3h and to Bruno Canard for the plasmid expressing the dengue virus NS3 helicase.

REFERENCES

1. **Abdel-Megeed AM, Abdel-Rahman HM, Alkaramany GE, El-Gendy MA.** 2009. Design, synthesis and molecular modeling study of acylated 1,2,4-triazole-3-acetates with potential anti-inflammatory activity. Eur. J. Med. Chem. **44**:117–123.
2. **Adedeji AO, et al.** 2012. Mechanism of nucleic acid unwinding by SARS-CoV helicase. PLoS One **7**:e36521. doi:10.1371/journal.pone.0036521.

2a. **Ahnert P, Patel SS.** 1997. Asymmetric interactions of hexameric bacteriophage T7 DNA helicase with the 5′- and 3′-tails of the forked DNA substrate. J. Biol. Chem. **272**:32267–32273.

3. **Ali JA, Lohman TM.** 1997. Kinetic measurement of the step size of DNA unwinding by Escherichia coli UvrD helicase. Science **275**:377–380.
4. **Almazan F, et al.** 2006. Construction of a severe acute respiratory syndrome coronavirus infectious cDNA clone and a replicon to study coronavirus RNA synthesis. J. Virol. **80**:10900–10906.
5. **Anand K, Ziebuhr J, Wadhwani P, Mesters JR, Hilgenfeld R.** 2003. Coronavirus main proteinase (3CLpro) structure: basis for design of anti-SARS drugs. Science **300**:1763–1767.
6. **Benarroch D, et al.** 2004. The RNA helicase, nucleotide 5′-triphosphatase, and RNA 5′-triphosphatase activities of dengue virus protein NS3 are Mg2+-dependent and require a functional Walker B motif in the helicase catalytic core. Virology **328**:208–218.
7. **Borowski P, Schalinski S, Schmitz H.** 2002. Nucleotide triphosphatase/helicase of hepatitis C virus as a target for antiviral therapy. Antiviral Res. **55**:397–412.
8. **Castro C, et al.** 2009. Nucleic acid polymerases use a general acid for nucleotidyl transfer. Nat. Struct. Mol. Biol. **16**:212–218.
9. **Chen J, et al.** 2007. Synthesis and anticonvulsant evaluation of 4-(4-alkoxylphenyl)-3-ethyl-4H-1,2,4-triazoles as open-chain analogues of 7-alkoxyl-4,5-dihydro[1,2,4]triazolo[4,3-a]quinolines. Bioorg. Med. Chem. **15**:6775–6781.
10. **Chen JY, et al.** 2009. Interaction between SARS-CoV helicase and a multifunctional cellular protein (Ddx5) revealed by yeast and mammalian cell two-hybrid systems. Arch. Virol. **154**:507–512.
11. **Cordin O, Banroques J, Tanner NK, Linder P.** 2006. The DEAD-box protein family of RNA helicases. Gene **367**:17–37.
12. **Crute JJ, et al.** 2002. Herpes simplex virus helicase-primase inhibitors are active in animal models of human disease. Nat. Med. **8**:386–391.
13. **D'Abramo CM, Archambault J.** 2011. Small molecule inhibitors of human papillomavirus protein-protein interactions. Open Virol. J. **5**:80–95.
14. **Durk RC, et al.** 2010. Inhibitors of foot and mouth disease virus targeting a novel pocket of the RNA-dependent RNA polymerase. PLoS One **5**:e15049. doi:10.1371/journal.pone.0015049.
15. **Eoff RL, Raney KD.** 2006. Intermediates revealed in the kinetic mechanism for DNA unwinding by a monomeric helicase. Nat. Struct. Mol. Biol. **13**:242–249.
16. **Fan K, et al.** 2004. Biosynthesis, purification, and substrate specificity of severe acute respiratory syndrome coronavirus 3C-like proteinase. J. Biol. Chem. **279**:1637–1642.
17. **Flores MJ, Sanchez N, Michel B.** 2005. A fork-clearing role for UvrD. Mol. Microbiol. **57**:1664–1675.
18. **Galletto R, Jezewska MJ, Bujalowski W.** 2004. Unzipping mechanism of the double-stranded DNA unwinding by a hexameric helicase: the effect of the 3′ arm and the stability of the dsDNA on the unwinding activity of the Escherichia coli DnaB helicase. J. Mol. Biol. **343**:101–114.
19. **Geider K, Hoffmann-Berling H.** 1981. Proteins controlling the helical structure of DNA. Annu. Rev. Biochem. **50**:233–260.
20. **Ivanov KA, et al.** 2004. Multiple enzymatic activities associated with severe acute respiratory syndrome coronavirus helicase. J. Virol. **78**:5619–5632.
21. **Jankowsky E, Gross CH, Shuman S, Pyle AM.** 2001. Active disruption of

an RNA-protein interaction by a DExH/D RNA helicase. Science **291**:121–125.
22. **Khalil NS.** 2006. Efficient synthesis, structure, and antimicrobial activity of some novel N- and S-beta-D-glucosides of 5-pyridin-3-yl-1,2,4-triazoles. Carbohydr. Res. **341**:2187–2199.
23. **Kim MK, et al.** 2011. 2,6-Bis-arylmethyloxy-5-hydroxychromones with antiviral activity against both hepatitis C virus (HCV) and SARS-associated coronavirus (SCV). Eur. J. Med. Chem. **46**:5698–5704.
24. **Kleymann G.** 2003. New antiviral drugs that target herpesvirus helicase primase enzymes. Herpes **10**:46–52.
25. **Kleymann G, et al.** 2002. New helicase-primase inhibitors as drug candidates for the treatment of herpes simplex disease. Nat. Med. **8**:392–398.
26. **Klimesova V, Zahajska L, Waisser K, Kaustova J, Mollmann U.** 2004. Synthesis and antimycobacterial activity of 1,2,4-triazole 3-benzylsulfanyl derivatives. Farmaco **59**:279–288.
27. **Kucukguzel I, et al.** 2004. Synthesis of some 3-(arylalkylthio)-4-alkyl/aryl-5-(4-aminophenyl)-4H-1,2,4-triazole derivatives and their anticonvulsant activity. Farmaco **59**:893–901.
28. **Kumamoto T, et al.** 1990. Effect of 2,4-dihydro-3H-1,2,4-triazole-3-thiones and thiosemicarbazones on iodide uptake by the mouse thyroid: the relationship between their structure and anti-thyroid activity. Chem. Pharm. Bull. (Tokyo) **38**:2595–2596.
29. **Kumar H, Javed SA, Khan SA, Amir M.** 2008. 1,3,4-Oxadiazole/thiadiazole and 1,2,4-triazole derivatives of biphenyl-4-yloxy acetic acid: synthesis and preliminary evaluation of biological properties. Eur. J. Med. Chem. **43**:2688–2698.
30. **Kwong AD, Rao BG, Jeang KT.** 2005. Viral and cellular RNA helicases as antiviral targets. Nat. Rev. Drug Discov. **4**:845–853.
31. **Lee C, et al.** 2009. Aryl diketoacids (ADK) selectively inhibit duplex DNA-unwinding activity of SARS coronavirus NTPase/helicase. Bioorg. Med. Chem. Lett. **19**:1636–1638.
32. **Lestini R, Michel B.** 2007. UvrD controls the access of recombination proteins to blocked replication forks. EMBO J. **26**:3804–3814.
33. **Levin MK, Patel SS.** 1999. The helicase from hepatitis C virus is active as an oligomer. J. Biol. Chem. **274**:31839–31846.
34. **Levin MK, Wang YH, Patel SS.** 2004. The functional interaction of the hepatitis C virus helicase molecules is responsible for unwinding processivity. J. Biol. Chem. **279**:26005–26012.
35. **Lipinski CA, Lombardo F, Dominy BW, Feeney PJ.** 2001. Experimental and computational approaches to estimate solubility and permeability in drug discovery and development settings. Adv. Drug Deliv. Rev. **46**:3–26.
36. **Lohman TM.** 1992. Escherichia coli DNA helicases: mechanisms of DNA unwinding. Mol. Microbiol. **6**:5–14.
37. **Lohman TM.** 1993. Helicase-catalyzed DNA unwinding. J. Biol. Chem. **268**:2269–2272.
38. **Lohman TM, Bjornson KP.** 1996. Mechanisms of helicase-catalyzed DNA unwinding. Annu. Rev. Biochem. **65**:169–214.
39. **Lucius AL, et al.** 2002. DNA unwinding step-size of E. coli RecBCD helicase determined from single turnover chemical quenched-flow kinetic studies. J. Mol. Biol. **324**:409–428.
40. **Marra MA, et al.** 2003. The genome sequence of the SARS-associated coronavirus. Science **300**:1399–1404.
41. **Masters PS.** 2006. The molecular biology of coronaviruses. Adv. Virus Res. **66**:193–292.
42. **Matson SW, Kaiser-Rogers KA.** 1990. DNA helicases. Annu. Rev. Biochem. **59**:289–329.
43. **Mouw MB, Pintel DJ.** 2000. Adeno-associated virus RNAs appear in a temporal order and their splicing is stimulated during coinfection with adenovirus. J. Virol. **74**:9878–9888.
44. **Ndongwe TP, et al.** 2012. Biochemical, inhibition and inhibitor resistance studies of xenotropic murine leukemia virus-related virus reverse transcriptase. Nucleic Acids Res. **40**:345–359.
45. **Nicholls JM, et al.** 2003. Lung pathology of fatal severe acute respiratory syndrome. Lancet **361**:1773–1778.
46. **Patel SS.** 2009. Structural biology: steps in the right direction. Nature **462**:581–583.
47. **Patel SS, Donmez I.** 2006. Mechanisms of helicases. J. Biol. Chem. **281**:18265–18268.
48. **Patel SS, Picha KM.** 2000. Structure and function of hexameric helicases. Annu. Rev. Biochem. **69**:651–697.
49. **Periyasamy-Thandavan S, et al.** 2012. Insulin-like growth factor 1 attenuates antiestrogen- and antiprogestin-induced apoptosis in ER+ breast cancer cells by MEK1 regulation of the BH3-only pro-apoptotic protein Bim. Breast Cancer Res. **14**:R52.
50. **Poutanen SM, et al.** 2003. Identification of severe acute respiratory syndrome in Canada. N. Engl. J. Med. **348**:1995–2005.
51. **Powdrill MH, Deval J, Narjes F, De Francesco R, Gotte M.** 2010. Mechanism of hepatitis C virus RNA polymerase inhibition with dihydroxypyrimidines. Antimicrob. Agents Chemother. **54**:977–983.
52. **Rota PA, et al.** 2003. Characterization of a novel coronavirus associated with severe acute respiratory syndrome. Science **300**:1394–1399.
53. **Sarafianos SG, Kortz U, Pope MT, Modak MJ.** 1996. Mechanism of polyoxometalate-mediated inactivation of DNA polymerases: an analysis with HIV-1 reverse transcriptase indicates specificity for the DNA-binding cleft. Biochem. J. **319**:619–626.
54. **Schoborg RV, Pintel DJ.** 1991. Accumulation of MVM gene products is differentially regulated by transcription initiation, RNA processing and protein stability. Virology **181**:22–34.
55. **Scholz I, et al.** 2009. Pharmacokinetics, metabolism and bioavailability of the triazole antifungal agent voriconazole in relation to CYP2C19 genotype. Br. J. Clin. Pharmacol. **68**:906–915.
56. **Seybert A, et al.** 2005. A complex zinc finger controls the enzymatic activities of nidovirus helicases. J. Virol. **79**:696–704.
57. **Sharma S, Doherty KM, Brosh RM, Jr.** 2005. DNA helicases as targets for anti-cancer drugs. Curr. Med. Chem. Anticancer Agents **5**:183–199.
58. **Singh K, Modak MJ.** 2003. Presence of 18-A long hydrogen bond track in the active site of Escherichia coli DNA polymerase I (Klenow fragment). Its requirement in the stabilization of enzyme-template-primer complex. J. Biol. Chem. **278**:11289–11302.
59. **Singh K, Srivastava A, Patel SS, Modak MJ.** 2007. Participation of the fingers subdomain of Escherichia coli DNA polymerase I in the strand displacement synthesis of DNA. J. Biol. Chem. **282**:10594–10604.
60. **Snijder EJ, et al.** 2003. Unique and conserved features of genome and proteome of SARS-coronavirus, an early split-off from the coronavirus group 2 lineage. J. Mol. Biol. **331**:991–1004.
61. **Tanner JA, et al.** 2003. The severe acute respiratory syndrome (SARS) coronavirus NTPase/helicase belongs to a distinct class of 5′ to 3′ viral helicases. J. Biol. Chem. **278**:39578–39582.
62. **Tanner JA, et al.** 2005. The adamantane-derived bananins are potent inhibitors of the helicase activities and replication of SARS coronavirus. Chem. Biol. **12**:303–311.
63. **Thiel V, et al.** 2003. Mechanisms and enzymes involved in SARS coronavirus genome expression. J. Gen. Virol. **84**:2305–2315.
64. **Tsang KW, et al.** 2003. A cluster of cases of severe acute respiratory syndrome in Hong Kong. N. Engl. J. Med. **348**:1977–1985.
65. **van Dinten LC, van Tol H, Gorbalenya AE, Snijder EJ.** 2000. The predicted metal-binding region of the arterivirus helicase protein is involved in subgenomic mRNA synthesis, genome replication, and virion biogenesis. J. Virol. **74**:5213–5223.
66. **van Hemert MJ, et al.** 2008. SARS-coronavirus replication/transcription complexes are membrane-protected and need a host factor for activity in vitro. PLoS Pathog. **4**:e1000054. doi:10.1371/journal.ppat.1000054.
67. **Veaute X, et al.** 2005. UvrD helicase, unlike Rep helicase, dismantles RecA nucleoprotein filaments in Escherichia coli. EMBO J. **24**:180–189.
68. **Veaute X, et al.** 2003. The Srs2 helicase prevents recombination by disrupting Rad51 nucleoprotein filaments. Nature **423**:309–312.
69. **von Brunn A, et al.** 2007. Analysis of intraviral protein-protein interactions of the SARS coronavirus ORFeome. PLoS One **2**:e459. doi:10.1371/journal.pone.0000459.
70. **Yang H, et al.** 2003. The crystal structures of severe acute respiratory syndrome virus main protease and its complex with an inhibitor. Proc. Natl. Acad. Sci. U. S. A. **100**:13190–13195.
71. **Yang N, et al.** 2007. Inhibition of SARS coronavirus helicase by bismuth complexes. Chem. Commun. (Camb.) **2007**:4413–4415.
72. **Zhang JH, Chung TD, Oldenburg KR.** 1999. A simple statistical parameter for use in evaluation and validation of high throughput screening assays. J. Biomol. Screen. **4**:67–73.
73. **Ziebuhr J, Snijder EJ, Gorbalenya AE.** 2000. Virus-encoded proteinases and proteolytic processing in the Nidovirales. J. Gen. Virol. **81**:853–879.